Available online at www.sciencedirect.com
ScienceDirect
Trans. Nonferrous Met. Soc. China 30(2020) 123−133
Transactions of Nonferrous Metals Society of China
www.tnmsc.cn

Zinc-doped hydroxyapatite−zeolite/polycaprolactone composites coating on magnesium substrate for enhancing in-vitro corrosion and antibacterial performance

Nida IQBAL[1], Saman IQBAL[2], Tanveer IQBAL[3], H. R. BAKHSHESHI-RAD[4], Ahmed ALSAKKAF[5], Ahmad KAMIL[6], Mohammed Rafiq ABDUL KADIR[7], Mohd Hasbullah IDRIS[5], H. Balaji RAGHAV[8]

1. Biomedical Engineering Centre, University of Engineering and Technology, Kala Shah Kaku (KSK) Campus, Lahore, Pakistan;
2. Department of Physics, University of the Punjab, Quaid-e-Azam Campus, Labore, Pakistan;
3. Department of Chemical Polymer & Composite Material Engineering, University of Engineering and Technology, Kala Shah Kaku (KSK) New Campus, Lahore, Pakistan;
4. Advanced Materials Research Center, Department of Materials Engineering, Najafabad Branch, Islamic Azad University, Najafabad, Iran;
5. School of Mechanical Engineering, Faculty of Engineering, Universiti Teknologi Malaysia, Johor, Malaysia;
6. Kulliyyah of Science, International Islamic University Malaysia, Bandar Indera Mahkota Campus, Jalan Sultan Ahmad Shah, 25200 Kuantan, Pahang Darul Makmur, Malaysia;
7. School of Biomedical Engineering and Health Sciences, Faculty of Engineering, Universiti Teknologi Malaysia, Johor, Malaysia;
8. Tissue Engineering Group (TEG), National Orthopaedic Centre of Excellence in Research and Learning (NOCERAL), Department of Orthopaedic Surgery, Faculty of Medicine, University of Malaya, 50603 Lembah Pantai, Kuala Lumpur, Malaysia

Received 8 April 2019; accepted 11 November 2019

Abstract: This work is focused on developing zinc-doped hydroxyapatite−zeolite (ZnHA−Zeo) and polycaprolactone (PCL) composite coatings on magnesium (Mg) substrate to improve the corrosion resistance and antimicrobial properties. Dip-coating technique was used to coat ZnHA−Zeo/PCL on the Mg substrate at room temperature. The samples were subjected to field emission scanning electron microscopy (FESEM), X-ray diffraction (XRD), Fourier transform infrared (FTIR), energy dispersive X-ray spectroscopy (EDX) and antimicrobial potential. Results demonstrated that composite coatings consist of HA, scholzite, zeolite, and PCL phases. EDX spectra indicated the presence of calcium (Ca), silicon (Si), aluminum (Al), zinc (Zn), phosphorus (P) and oxygen (O). The composite surface appeared in spherical-like microstructure on coating with thickness ranging 226−260 μm. Zinc-doped HA−Zeo composite coating had a high corrosion resistance and provided sufficient protection to the Mg surface against galvanic corrosion. Doped ZnHA−Zeo coating samples exhibited superior disc inhibition by confirming antimicrobial activity against the *E. coli* as compared to HA−Zeo sample. Altogether these results showed that the ZnHA−Zeo coatings not only improved the corrosion resistance, but also enhanced the antimicrobial property and hence they can be used as suitable candidates for implant applications.

Key words: biodegradable magnesium; bioceramics coating; corrosion resistance; antimicrobial activity

Corresponding author: Nida IQBAL; Tel: +92-3434172495; E-mail: nidaiqbal@uet.edu.pk
DOI: 10.1016/S1003-6326(19)65185-X

1 Introduction

Recently, biodegradable metals such as magnesium, iron, zinc and their alloys have gained considerable attention as suitable candidates for implant in orthopedic applications due to their low weight, biodegradability, non-toxicity, biocompatibility and superior mechanical characteristics [1−3]. These materials are implanted in the body for certain period until the healing process of bones is completed and they gradually start to dissolve, be absorbed or excreted. Therefore, unlike permanent implants, biodegradable implants do not need a second surgery for implant removal [4,5]. Despite many advantages, there are a few main drawbacks associated with the use of Mg for this purpose, i.e., high degradation rate in the biological environment, production of hydrogen bubbles, metal dissolution, and local alkalization [6−8]. Hence, improving the degradation rate of Mg is essential for ensuring the applications of Mg-based biomaterials. Several methods have been utilized in order to delay the rapid degradation of Mg which includes bulk alloying, mechanical deformation and surface modification [9−11]. However, elemental alloying could reduce the corrosion rate of Mg alloys, but it may lack biological activity by providing insufficient bone healing response [12,13].

Hence, the surface modification via bioactive coating has been gaining attention to improve the degradation rate and bioactivity of Mg and Mg alloys [14,15]. Bioactive coatings made of hydroxyapatite (HA) and polymeric materials have recently been used for orthopedic implant applications because their chemical and biological compositions are similar to those of the natural bone [16,17]. Among the various biodegradable polymers, PCL is considered as a promising candidate for metallic implant coating due to its excellent biocompatibility, biodegradability structural stability and mechanical properties. An addition advantage of PCL is that coating does not need post-depositional heat treatment for densification. Furthermore, the addition of zeolites (Zeo) into HA may help in improving the corrosion resistance and mechanical properties of implants [18]. However, HA showed poor antibacterial performance which may lead to bacterial infection during the implantation process [19,20]. To overcome these issues, a combination of antibacterial metals (Ag, Zn, Ti, Cu, etc) has been utilized to develop biomaterial composites that can improve the bioactivity and decrease the risk of post-operative infections. It has been observed that doping of metal ions such as Zn, Sr, Cu, Ag, Zr, Sn and Ti into HA lattices not only offers antimicrobial property, but also improves crystalline structure [21−23]. Among various metals, the incorporation of zinc in HA lattice has the ability to stimulate bone mineralization, cell proliferation and antimicrobial properties [24,25].

Among various surface coating techniques such as thermal spray, electrodeposition, and laser cladding [26], dip coating technique is found an effective method of preparing a wide range of surfaces for biocompatible and bioactive materials. Main advantages of dip coating include simplicity, being inexpensive, efficiently controlling the coating parameters and being able to coat complex shaped designs [27−29]. Until now, bioactivity, corrosion behavior, and antimicrobial performance of the ZnHA−Zeo coating have less been reported.

In this work, bioceramics−polymer composites coating was prepared on magnesium substrates, with the aim of controlling the rate of corrosion and improving antibacterial performance. Dip coating method was used to coat ZnHA−Zeo/PCL composites on Mg substrate along with their chemical and microstructural analysis. Furthermore, the corrosion behavior was studied using Tafel and EIS methods. Then, antimicrobial response of prepared coatings was evaluated by disc diffusion and spread plate methods.

2 Experimental

2.1 Synthesis of zinc-incorporated HA

Hydroxyapatite containing zinc nanoparticles were synthesized by substituting Ca with Zn according to a well-established microwave method [30]. For this reaction, two substitution values of zinc ions into the calcium ions in HA were selected which were x=0.4 and 0.8 (according to $Ca_{10-x}Zn_x(PO_4)_6(OH)_2$) (Eq. (1)):

$$(10-x)Ca^{2+}+xZn^{2+}+PO_4^{3-}+2OH^- \rightarrow Ca_{10-x}Zn_x(PO_4)_6(OH)_2 \quad (1)$$

Briefly, an aqueous solution of calcium nitrate

(CaN) and zinc nitrate (ZnN) was prepared by maintaining molar concentration of Zn+Ca at 1 mol/L. Subsequently, 0.6 mol/L diammonium hydrogen phosphate solution was added dropwise to the Ca+Zn solution, and the pH of the mixture was maintained at 10. The reaction mixture was then refluxed under microwave radiation (Samsung-MW71B, 800 W, 2.45 GHz) for 10 min. All samples were filtered, dried and sintered at 1000 °C.

2.2 Sample preparation

Pure magnesium samples (99.80%) were cut from cast ingot into small plate sample using wire cutter machine with a dimension of 1.5 cm × 1.5 cm × 0.2 cm, and mechanically ground with 1000# silicon paper. Subsequently, samples were rinsed with acetone in ultrasonic bath for 15 min and dried using compressed air.

2.3 Deposition of HA−Zeo/PCL and ZnHA−Zeo/PCL on Mg plate samples

Bioceramics−polymer composite coatings (75 wt.% HA−Zeo or *n*ZnHA−Zeo and 25 wt.% PCL) were applied on top of the Mg plates via dip coating method, as shown in Fig. 1.

Briefly, 1.5 g of polycaprolactone pallet (M_w= 80×10^3 g/mol, Sigma-Aldrich, UK) was added to 20 mL chloroform (QRëCTM, AR grade) followed by the addition of corresponding amounts of HA powder (3.3 g) and zeolite (Sigma-Aldrich, UK) (1.2 g) at room temperature. The resultant suspension was stirred for 6 h to produce the homogenous mixture. Same procedure was repeated for the preparation of *n*ZnHA−Zeo/PCL slurries.

The deposition of Mg was conducted in homogeneous suspension using a dip coater (HTWL−01 Desktop, MT1 Cooperation, USA) at room temperature. The Mg substrate was coated 3 times in the slurry. At each time, the plate sample was dipped in the slurry for 2 min and allowed to be dried for 2 min. During each interval of drying, the slurry was put back to hot stirrer to prevent it from coagulating. Then, the coated samples were dried in the oven at 50 °C.

2.4 Sample characterization

Microstructure analysis was done using a scanning electron microscope (JEOL JSM−6380LA) equipped with EDS analysis. Coating thickness was estimated by cross-sectional FE-SEM observation of the coated specimens. An X-ray diffractometer (Siemens−D5000) was used to analyze the phase composition of the coated samples by using Cu K_α radiation (λ=1.5405 Å) generated at 35 kV and 25 mA. Characteristic functional groups in the powder samples were identified by FTIR Bruker (Optic GmbH) ALPHA-T. A finely divided powder sample was mixed with potassium bromide (KBr) powder and pressed into a die to make a transparent pellet. Spectra were recorded over the region 400−4000 cm^{-1}.

2.5 Electrochemical impedance measurements

For electrochemical analysis, rectangular Mg specimens (1 cm^2 surface area) were mounted into an epoxy resin. The test was performed in an open-air glass cell containing 350 mL Kokubo simulated body fluid (SBF) solution [31] with pH of 7.44 at 37 °C using potentiostat/galvanostat

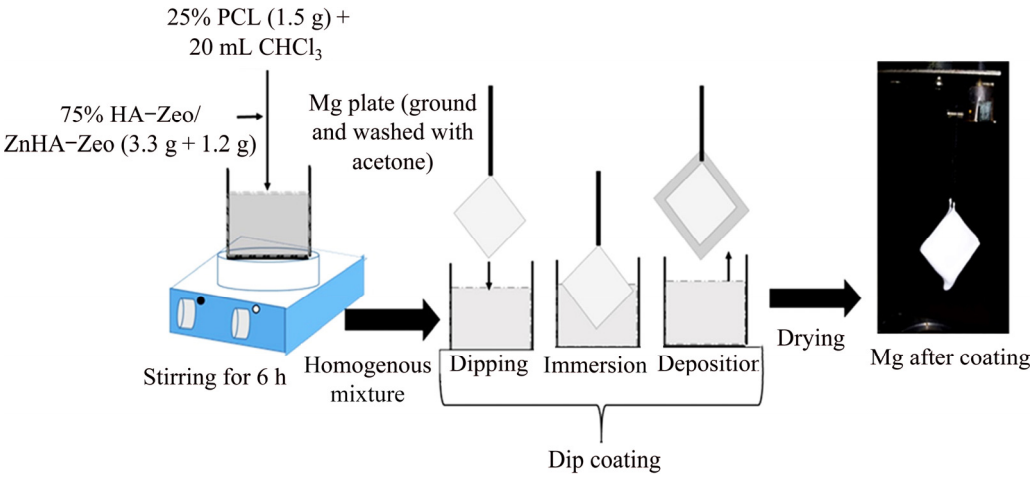

Fig. 1 Schematic diagram of dip coating technique

(PARSTAT 2263, Princeton Applied Research). A three-electrode cell was used in which the specimen with exposed area of 0.4 cm^2 was used as a working electrode, a saturated calomel electrode (SCE) acted as a reference electrode, and the graphite rod was used as counter electrode. The samples were immersed in the SBF for 1 h prior to the potentiodynamic polarization (PDP) test to establish the open-circuit potential for providing uniform corrosion and well-defined Tafel region. All electrochemical analyses were performed at a constant scan rate (0.5 mV/s) that was initiated at −250 mV below the open-circuit potential. Electrochemical impedance spectroscopy was performed in the frequency range from 100 kHz to 0.01 Hz with 10 points per decade and 10 mV. The Zsimp Win software was used to analyze the data. Each electrochemical experiment was duplicated to observe the reproducibility of the results.

2.6 Antibacterial testing

The antibacterial activities of HA−Zeo and ZnHA−Zeo coated samples were evaluated using the agar disk-diffusion technique and spread plate method. Nutrient agar plate (NA plate) and Luria−Bertani broth (LB broth) were prepared as a medium for antibacterial testing. Stock solution for each organism (1×10^8 CFU/mL) was prepared by mixing 20 mL of the culture bacteria solution with 180 mL of LB broth and incubated at 37 °C for 24 h with shaking at 200 r/min. For disk diffusion, a drop of subculture bacteria was placed at the center of the NA plate. The subculture bacteria were spread using the cotton bud on each quadrant. Then, the coated samples were placed in the center of the NA plate. Lastly, the NA plate was sealed with parafilm and incubated at 37 °C for 24 h.

3 Results and discussion

3.1 Microstructure and composition

The surface morphology of HA−Zeo, 1ZnHA−Zeo and 2ZnHA−Zeo coating was observed using FESEM, as shown in Fig. 2. At a low magnification,

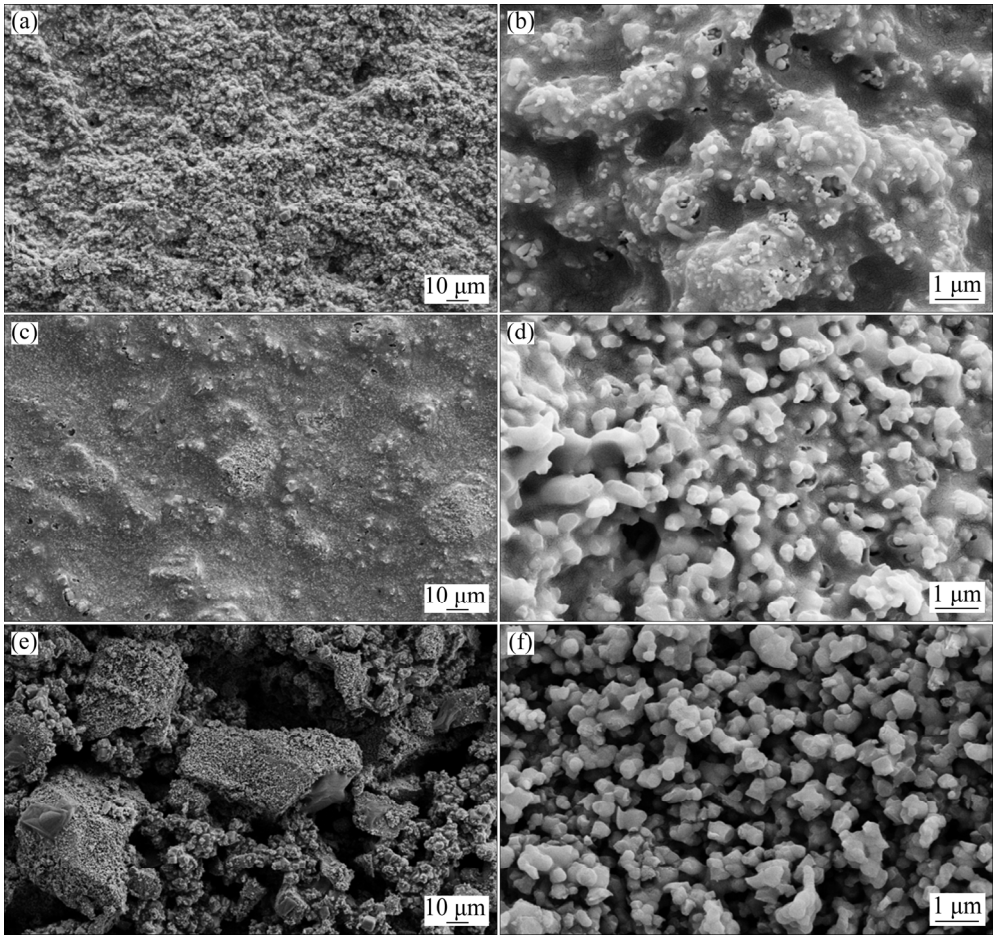

Fig. 2 FESEM images of composite coatings: (a, b) HA−Zeo; (c, d) 1ZnHA−Zeo; (e, f) 2ZnHA−Zeo

it was observed that the HA−Zeo coating had a rough and dense surface with randomly distributed particles. The addition of Zn into HA coating induced particle segregation and the formation of agglomeration at surface level pores. The size of the agglomerates tended to increase as the amount of zinc increased, as shown in Figs. 2(c, e). Furthermore, it was observed that the HA coating consisted of elongated spherical particles which were tightly agglomerated into microscale aggregates, as shown in Fig. 2(b). Although ZnHA−Zeo images showed the aggregation of particles with increased spaces among the particles, it had a smooth coating. Voids on the surface confirmed partly porous nature of the material, as shown in Figs. 2(d, f). The nature of this porous microstructure could be beneficial as the nucleation rate of HA on the coating surface was improved and hence, the bioactivity of the prepared porous coating may be superior [32]. Therefore, it was reasonable to state that the porous feature of coatings was desirable and might accelerate the precipitation of apatite on the coatings.

Figures 3(a, c, e) show the cross-sectional surfaces of the composite coatings, which indicated that the surface was smooth and uniform on the Mg without any delamination and crack at the interface. The average thicknesses of HA−Zeo, 1ZnHA−Zeo and 2ZnHA−Zeo were observed to be (226±0.2), (251±0.2) and (260±0.2) μm, respectively. The increment in layer thickness might be due to the effect of surface wettability of the substrate and the bottom 2ZnHA−Zeo layer. These results suggested that the dip coating technique had the capability to deposit thick coatings so as to overcome the problems associated with plasma-sprayed thick (>100 μm) coatings. This EDS pattern confirmed the presence of Ca, Si, Al, Zn, P and O on the coating surface, as shown in Figs. 3(b, d, f).

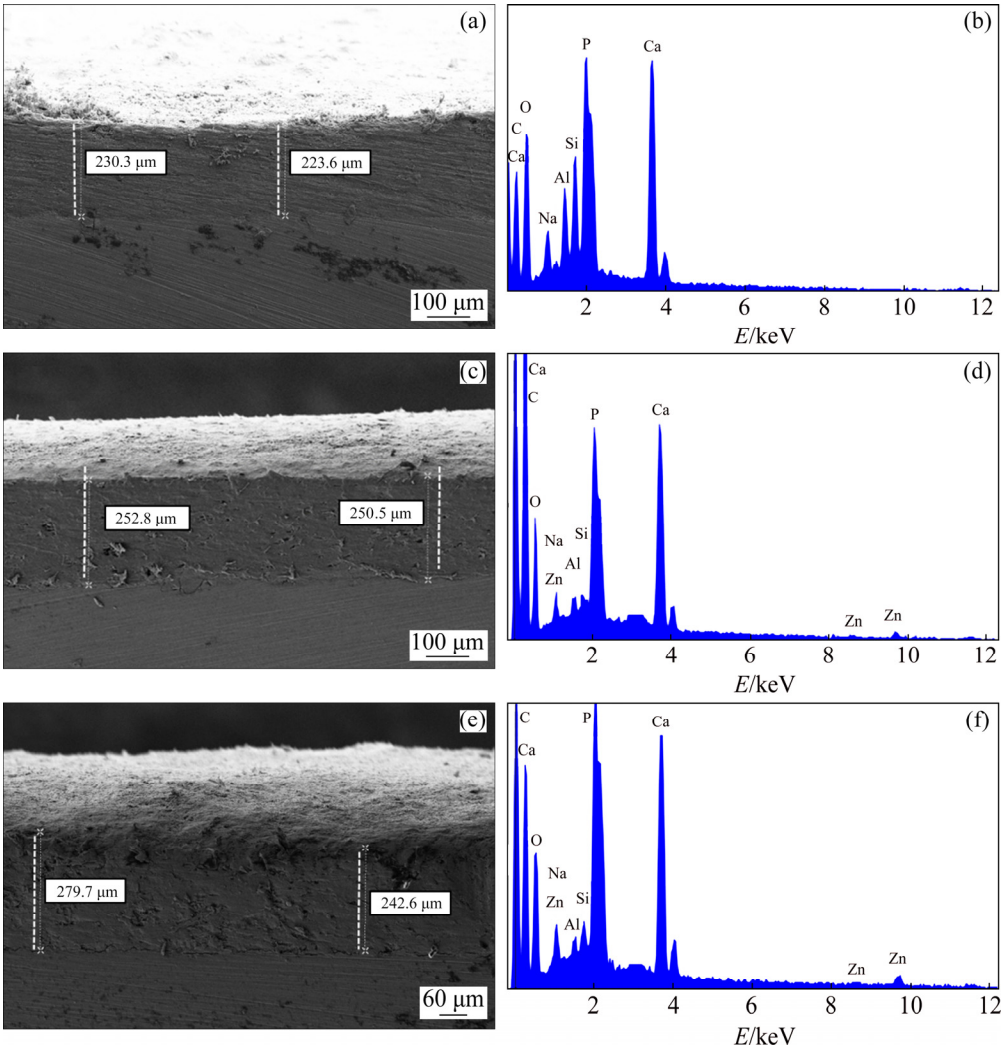

Fig. 3 Cross-sectional FESEM images (a, c, e) and EDS spectra (b, d, f) of composite coatings: (a, b) HA−Zeo; (c, d) 1ZnHA−Zeo; (e, f) 2ZnHA−Zeo

3.2 FTIR and XRD analysis

The incorporation of HA−Zeo, 1ZnHA−Zeo and 2ZnHA−Zeo coating was evaluated by FTIR and XRD analyses. Figure 4 presents the XRD patterns of HA−Zeo, 1ZnHA−Zeo and 2ZnHA−Zeo samples recorded in the 2θ range of 10°−60°. The XRD patterns of all samples showed the presence of HA peaks at 2θ=26.5°, 31.9°, 32.8°, 34.2°, 39.8°, 47.7° and 49.5° which are in agreement with those of XRD JCPDs data file No. 09-432 corresponding to crystalline HA. Whereas, the peaks at 2θ=17.09°, 21.95°, 25.9°, 27.96°, 31.15°, 34.57° and 53.80° corresponded to the Zeo (compared to ICDD patterns 42-0023). The peaks at 2θ=21.45° and 23.76° indicated the presence of PCL in composite coatings [33]. In the case of 1ZnHA−Zeo and 2ZnHA−Zeo, a peak at 35.6° represented scholzite $CaZn_2(PO_4)_2{\cdot}2H_2O$ (JCPDS 35-0495). Furthermore, β-TCP phase was also found in the XRD patterns at 2θ=31.17° and 34.5° (compared to ICDD patterns 09-0169). The presence of low-intensity peaks indicated the low crystallinity in the composite coatings. Thus, the XRD analysis indicated that the addition of metal ions and Zeo affected the HA crystal structure, stability, and thermal decomposition and produced an inhibitory effect on HA formation. The presence of other phases is in agreement with the XRD results, indicating a successful addition of ions into HA−Zeo composites.

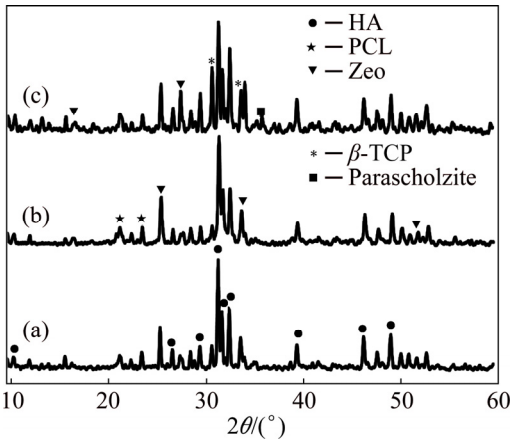

Fig. 4 XRD patterns of coated specimens: (a) HA−Zeo; (b) 1ZnHA−Zeo; (c) 2ZnHA−Zeo

Figure 5 shows FTIR spectra of HA−Zeo, 1ZnHA−Zeo and 2ZnHA−Zeo coating. FTIR results showed peaks corresponding to crystalline HA, Zeo, PCL phases, respectively. In detail, the characteristic peaks for HA were observed at 1032 (1092), 963, 561 and 606 cm^{-1} representing asymmetric, symmetric and bending mode of P—O bond in phosphate group. Moreover, hydroxyl group stretching and libirational peaks were observed at 3572 and 632 cm^{-1}. In addition, characteristic peaks for PCL were found at 1721, 2865 and 2944 cm^{-1} that belonged to stretching and symmetric mode of C═O, asymmetric CH_2 stretching, respectively. Peaks found at 1160, 1239 and 1294 cm^{-1} assigned to C—O—C symmetric and asymmetric, C—O and C—C stretching bands. Meanwhile, the peaks that appeared at 1275, 972 and 464 cm^{-1} were assigned to the asymmetric stretching vibration of Si—Al—O, both Si—O—Si and Si—O—Al asymmetric stretching modes and Si—O—Si bending mode. However, few Zeo vibrations such as Si—O stretch at 1094 cm^{-1} and Si—O symmetric stretch at 963 cm^{-1} were difficult to identify due to the overlapping of phosphate absorption bands. Although there were no obvious changes in the absorption of phosphate, Zeo group bands were observed with the addition of zinc ions. However, the changes were observed in the hydroxyl vibration such as decreased intensity of OH libirational mode in HA. From these changes, it can be concluded that zinc ions substituted can cause the formation of β-TCP. These results are inconsistent with the XRD results, which also showed structural changes in HA with an increase in the Zn content in the range of 2.5−5 wt.%.

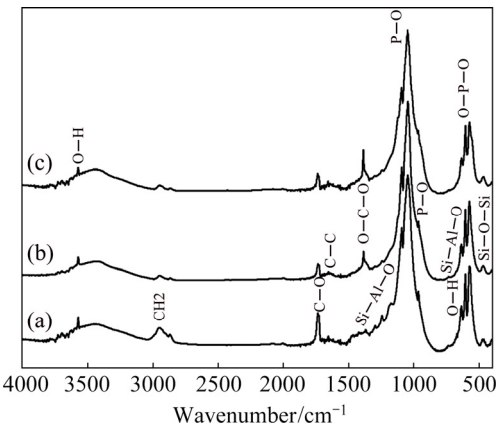

Fig. 5 FTIR spectra of coated specimens: (a) HA−Zeo; (b) 1ZnHA−Zeo; (c) 2ZnHA−Zeo

3.3 Electrochemical studies

Figure 6 shows the polarization curves for the uncoated Mg sample and Mg sample coated with the HA−Zeo, 1ZnHA−Zeo and 2ZnHA−Zeo, and

the corresponding kinematics parameters are summarized in Table 1. The corrosion potential was −1.925 V for bare Mg while the corrosion potential values were calculated to be −1.765, −1.701 and −1.634 V for Mg samples coated with HA−Zeo, 1ZnHA−Zeo and 2ZnHA−Zeo, respectively. This shift in φ_{corr} values to nobler values indicated that excellent protection was obtained through coating. It can also be seen that the decrease of corrosion current density (J_{corr}) of the uncoated sample was 95.59×10^{-3} mA/cm^2 and significant decrease was observed in J_{corr} for HA−Zeo, 1ZnHA−Zeo and 2ZnHA−Zeo to 84.67×10^{-3}, 25.76×10^{-3} and 10.32×10^{-3} mA/cm^2, respectively, which indicated a decrease in degradation rate for coated sample compared to bare Mg. The corrosion rate (P_i) of the samples, obtained from the corrosion current density, was calculated according to [34]

$$P_i=22.85J_{corr} \quad (1)$$

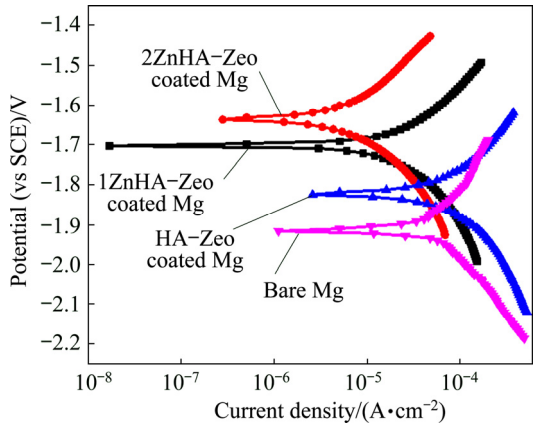

Fig. 6 Potentiodynamic polarization curves of bare Mg, HA−Zeo, 1ZnHA−Zeo and 2ZnHA−Zeo coated samples in Kokubo solution at 37 °C

Table 1 Electrochemical parameters of uncoated Mg, HA−Zeo, ZnHA−Zeo and 2ZnHA−Zeo coated samples in Kokubo solution obtained from polarization test

Sample	Corrosion Potential (vs SCE), φ_{corr}/mV	Current density, J_{corr}/(μA·cm^{-2})	Corrosion rate, P_i/(mm·a^{-1})
Bare Mg	−1925	95.59	2.184
HA−Zeo coated Mg	−1765	84.67	1.934
1ZnHA−Zeo coated Mg	−1701	25.76	0.588
2ZnHA−Zeo coated Mg	−1634	10.32	0.235

The corrosion rates of bare Mg, HA−Zeo, 1ZnHA−Zeo and 2ZnHA−Zeo coated Mg samples were 2.184, 1.934 to 0.588 and 0.235 mm/a, respectively. It can be seen that the presence of Zn in the coating may decrease the corrosion rate. The reason that 2ZnHA−Zeo coated sample has the lowest degradation rate is due to its thicker layer of coating which provides more protection to the substrate and acts as barrier against the corrosive attack of the chloride solutions [35]. Secondly, the roughness of coating also influenced the corrosion rate. HA coated sample has more rough coating surface compared to 1ZnHA−Zeo and 2ZnHA−Zeo coated sample. The larger the roughness of the coating, the more the exposed area to the solution, which results in accelerating the degradation rate of the coating [36].

Electrochemical impedance spectroscopy (EIS) was performed in Kokubo solution to assess the corrosion protective nature of HA−Zeo, 1ZnHA−Zeo and 2ZnHA−Zeo coatings. Figure 7(a) shows Nyquist curve of coated and uncoated samples. It is obvious that both the coated and uncoated samples had a capacitive loop in the high frequency range. A single capacitive loop was presented by 1ZnHA−Zeo and 2ZnHA−Zeo coated and bare Mg whereas two capacitive loops were presented by HA−Zeo coated sample. The presence of two capacitive loops with a smaller diameter compared to 1ZnHA−Zeo and 2ZnHA−Zeo indicated poor resistance of HA−Zeo coating. It can be seen that the loop of 2ZnHA−Zeo and 1ZnHA−Zeo coating had a larger diameter compared to the HA−Zeo coated and uncoated Mg samples, which indicated high resistance of these coatings. The high corrosion resistance of ZnHA−Zeo was due to the presence of dense and thick coating layer that can effectively provide protection against Mg degradation. It has been observed that the higher frequency capacitive loop may also due to the relaxation process of electrochemical impedance, which results in the dissolution of Mg and the electric double layer capacitance (Cdl) at electrode/electrolyte interface [37].

The Bode plot in Fig. 7(b) shows the low frequency impedance values for bare Mg and coated Mg samples. As can be seen, there were no significant difference in the values of the low frequency impedance of the uncoated and HA coated samples, whereas 2ZnHA−Zeo coated

sample showed higher impedance at low frequencies among all samples. Generally, higher impedance modulus at lower frequency indicates a higher corrosion resistance of sample [38]. Accordingly, the highest impedance values at lower frequency of 2ZnHA−Zeo and 1ZnHA−Zeo coated samples indicated a lower corrosion rate compared to those of HA−Zeo coated and uncoated Mg samples. These results are in match with the results that were obtained from polarization test. These data further confirmed that the presence of ZnHA composite improved the surface protection compared to bare Mg and the HA−Zeo coated samples.

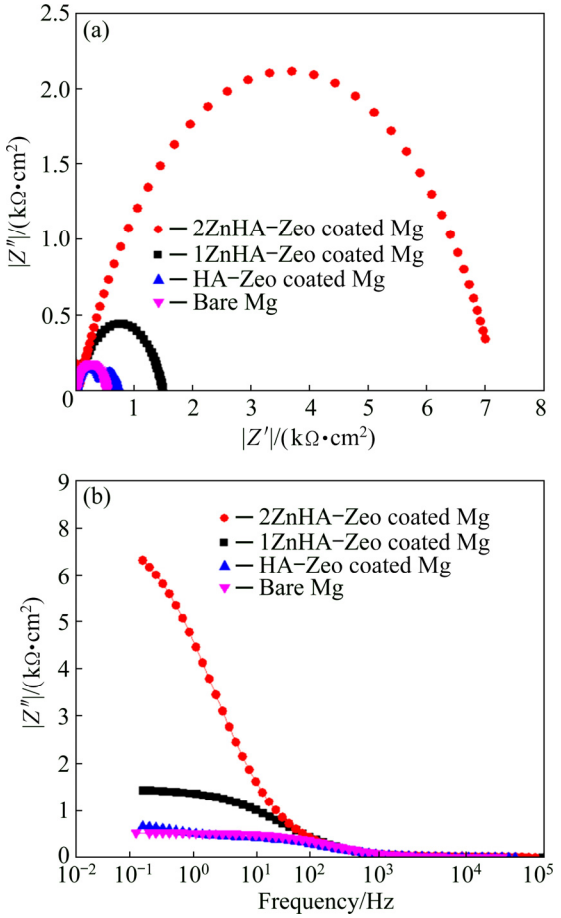

Fig. 7 Electrochemical impedance spectroscopy (EIS) measurement of bare Mg, HA−Zeo, 1ZnHA−Zeo and 2ZnHA−Zeo coated samples in Kokubo solution at 37 °C: (a) Nyquist plot; (b) Bode plot

3.4 Antimicrobial evaluation

The antimicrobial activities of coated samples were assessed using the disk diffusion and colony counting methods. Figure 8(a) shows the inhibition zones for *E. coli*. No inhibition zone for HA−Zeo coated samples was found, although the inhibition zones were observed around the coating containing Zn ions and the average inhibition zone for 1ZnHA−Zeo is (2.2±0.1) cm and for 2ZnHA−Zeo is (2.5±0.1) cm. Spread plate results in Fig. 8(b) indicated that HA−Zeo showed well-spread bacterial growth. Whereas, 2ZnHA−Zeo showed fewer colonies of bacteria grown compared to 1ZnHA−Zeo which were 14 colonies and 49 colonies, respectively. 2ZnHA−Zeo showed significant antibacterial effect, which may be due to the larger amount of zinc. These antibacterial results are in accordance with the previous observations [30], which indicated that Zn ions were bound to the DNA of bacteria, thereby preventing their replication or inactivation of a bacterial protein. Therefore, it can be concluded that doping of zinc into HA can help in resisting bacterial growth effectively.

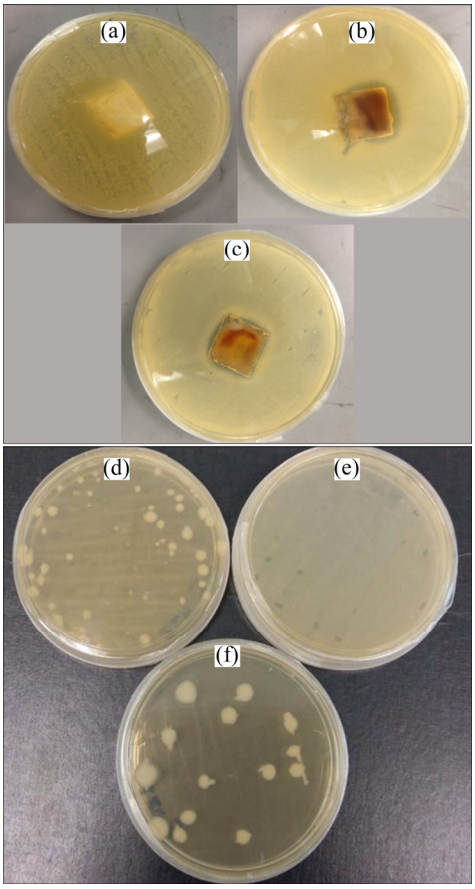

Fig. 8 Agar disk-diffusion (a, b, c) and spread plate (d, e, f) results of coated specimens against *E. coli* bacterial for 24 h: (a, d) HA−Zeo; (b, e) 1ZnHA−Zeo; (c, f) 2ZnHA−Zeo

In this study, the method proposed has following advantages such as low cost dip coating

method used to coat the Mg substrate at room temperature, and usage of PCL to eliminate the post-depositional heat treatment for densification. Zinc ions were used as antibacterial agent which significantly improved anti-bacterial properties besides biocompatibility and bioactivity. In comparison to the similar study reported (BAKHSHESHI-RAD et al [19]), the silver−zeolite doped hydroxyapatite (Ag−Zeo−HAP) coating on TiO_2-coated Mg alloy by physical vapour deposition (PVD) assisted electrodeposition technique which was very expensive and time consuming process, and gave thin coating (15 μm). Secondly, Ag ions are used which have good antibacterial property at high concentration, and they cause toxicity to the cell. Hence, our method outperforms it in these criteria, therefore zinc-doped hydroxyapatite−zeolite/polycaprolactone composite coatings on Mg are safe and promising for medical implant applications.

4 Conclusions

(1) ZnHA−Zeo/PCL composite coatings were successfully done on Mg substrate by dip coating method.

(2) XRD, FTIR and EDX spectra confirmed that composite coatings consisted of zinc-doped hydroxyapatite, zeolite, and PCL. From the FESEM analysis, it was found that the composite coatings were composed of spherical-like microstructure with thickness ranging 226−260 μm.

(3) In vitro corrosion results indicated that the composite coatings showed better corrosion resistance as compared to the bare Mg.

(4) ZnHA−Zeo surfaces were able to reduce the viability of adhered bacteria colonies as compared to HA−Zeo due to the existence of zinc in the coating.

(5) It could be concluded that a combination of Zn-doped HA and zeolite is a promising alternative to control the degradation rate of Mg while reduce the adhesion of viable bacteria to biomaterials.

(6) Our method does not take into the account the cell culture testing for the samples. Therefore, based on these findings, the future scope of the work would be to rigorously carry out various bio-compatibility tests to investigate the performance of composite coatings as implant applications.

Acknowledgments

This work was supported by University of Engineering and Technology, Lahore, faculty under research project # ORIC/102-ASRB/1288 and UTM, FRGS grant # R. J130000.7845.4F768.

References

[1] LI N, ZHENG Y. Novel magnesium alloys developed for biomedical application: A review [J]. Material Science and Technology, 2013, 29: 489−502.

[2] ZHEN Z, XI T F, ZHENG Y F. A review on in vitro corrosion performance test of biodegradable metallic materials [J]. Transactions of Nonferrous Metals Society of China, 2013, 23(8): 2283−2293.

[3] LIU Y, ZHENG Y, CHEN X H, YANG J A, PAN H, CHEN D, WANG L, ZHANG J, ZHU D, WU S, YEUNG K W K, ZENG R C, HAN Y, GUAN S. Fundamental theory of biodegradable metals— Definition, criteria, and design [J]. Advanced Functional Materials, 2019, 29(18):1805402.

[4] MUTLU I. Production and fluoride treatment of Mg−Ca−Zn−Co alloy foam for tissue engineering applications [J]. Transactions of Nonferrous Metals Society of China, 2018, 28(1): 114−124.

[5] WAN P, TAN L, YANG K. Surface modification on biodegradable magnesium alloys as orthopedic implant materials to improve the bio-adaptability: A review [J]. Journal of Material Science and Technology, 2016, 32: 827−834.

[6] ZHENG Y F, GU X N, WITTE F. Biodegradable metals [J]. Journal of Materials Science and Engineering R, 2014, 77: 1−34.

[7] XIN Y, HUB T, CHU P K. In vitro studies of biomedical magnesium alloys in a simulated physiological environment: A review [J]. Acta Biomaterials, 2011, 7: 1452−1459.

[8] RADHA R, SREEKANTH D. Insight of magnesium alloys and composites for orthopedic implant applications — A review [J] Journal of Magnesium Alloys, 2017, 5: 286−312.

[9] ABOUDZADEH N, DEHGHANIAN C, SHOKRGOZAR M A. In vitro degradation and cytotoxicity of Mg−5Zn−0.3Ca/nHA biocomposites prepared by powder metallurgy [J]. Transactions of Nonferrous Metals Society of China, 2018, 28(9): 1745−1754.

[10] GONZALEZ J, HOU R Q, NIDADAVOLU E P S, WILLUMEIT-RÖMER R, FEYERABEND F. Magnesium degradation under physiological conditions—Best practice [J]. Bioactive Materials, 2018, 3: 174−185.

[11] LI L Y, CUI L Y, ZENG R C, LI S Q, CHEN X B, ZHENG Y, KANNAN M B. Advances in functionalized polymer coatings on biodegradable magnesium alloys—A review [J]. Acta Biomaterialia, 2018, 79: 23−36.

[12] LI L Y, CUI L Y, LIU B, ZENG R C, CHEN X B, LI S Q, WANG Z L, HAN E H. Corrosion resistance of glucose-induced hydrothermal calcium phosphate coating on pure magnesium [J]. Applied Surface Science, 2019, 465: 1066−1077.

[13] JIA Q G, ZHANG W X, SUN Y, XU C X, ZHANG J S, KUAN J. Microstructure and mechanical properties of as-cast and extruded biomedical Mg−Zn−Y−Zr−Ca alloy at different temperatures [J]. Transactions of Nonferrous Metals Society of China, 2019, 29(3), 515−525.

[14] ZHANG L C, XU M, HU Y D, GAO F, GONG T, LIU T, LI X. Biofunctionization of biodegradable magnesium alloy to improve the in vitro corrosion resistance and biocompatibility [J]. Applied Surface Science, 2018, 451: 20−31.

[15] LIU P, WANG J M, YU X T, CHEN X B, LI S Q, CHEN D C, GUAN S K, ZENG R C, CUI L Y. Corrosion resistance of bioinspired DNA-induced Ca−P coating on biodegradable magnesium alloy [J]. Journal of Magnesium and Alloys, 2019, 7: 144−154.

[16] JI X J, CHENG Q, WANG J, ZHAO Y B, HAN Z Z, ZHANG F, LI S Q, ZENG R C, WANG Z L. Corrosion resistance and antibacterial effects of hydroxyapatite coating induced by polyacrylic acid and gentamicin sulfate on magnesium alloy [J]. Frontiers of Materials Science, 2019, 13: 87−98.

[17] YU C, CUI L Y, ZHOU Y B, HAN Z Z, CHEN X B, ZENG R C, ZOU Y H, LI S Q, ZHANG F, HAN E H, GUAN S K. Self- degradation of micro-arc oxidation/chitosan composite coating on Mg−4Li−1Ca alloy [J]. Surface and Coatings Technology, 2018, 344: 1−11.

[18] KE C, SONG M S, ZENG R C, QIU Y, ZHANG Y, ZHANG R F, LIU R L, COLE I, BIRBILIS N, CHEN X B. Interfacial study of the formation mechanism of corrosion resistant strontium phosphate coatings upon Mg−3Al−4.3Ca−0.1Mn [J]. Corrosion Science, 2019, 151: 143−153.

[19] BAKHSHESHI-RAD H R, HAMZAH E, ISMAIL A F, AZIZ M, KARAMIAN E, IQBAL N. Bioactivity, in-vitro corrosion behavior, and antibacterial activity of silver−zeolites doped hydroxyapatite coating on magnesium alloy [J]. Transactions of Nonferrous Metals Society of China, 2018, 28(8): 1553−1562.

[20] JI X J, GAO L, LIU J C, WANG J, CHENG Q, LI J P, LI S Q, ZHI K Q, ZENG R C, WANG Z L. Corrosion resistance and antibacterial properties of hydroxyapatite coating induced by gentamicin-loaded polymeric multilayers on magnesium alloys [J]. Colloids and Surfaces B: Biointerfaces, 2019, 179(1): 429−436.

[21] ZHAO Y, CHEN X, LI S Q, ZENG R, ZHANG F, WANG Z, GUAN S. Corrosion resistance and drug release profile of gentamicin-loaded polyelectrolyte multilayers on magnesium alloys: Effects of heat treatment [J]. Journal of Colloid & Interface Science, 2019, 547: 309−317.

[22] IQBAL N, KADIR M R A, MAHMOOD N H, IQBAL S, ALMASI D, NAGHIZADEH F, RAGHAVENDRAN H, KAMARUL T. Characterization and biological evaluation of silver containing fluoroapatite nanoparticles prepared through microwave synthesis [J]. Ceramics International, 2015, 41: 6470−64.

[23] DAROONPARVAR M, YAJID M A M, GUPTA R K, YUSOF N M, BAKHSHESHI-RAD H R, GHANDVAR H, GHASEMI E. Antibacterial activities and corrosion behavior of novel PEO/ nanostructured ZrO_2 coating on Mg alloy [J]. Transactions of Nonferrous Metals Society of China, 2018, 28(8): 1571−1581.

[24] KAWASHITA M, IWABUCHI Y, SUZUKI K, FURUYA M, YOKOTA K, KANETAKA H. Surface structure and in vitro apatite-forming ability of titanium doped with various metals [J]. Colloids and Surfaces A: Physicochemical and Engineering Aspects, 2018, 555: 558−564.

[25] UYSAL I, SEVERCAN F, TEZCANER A, EVIS Z. Co-doping of hydroxyapatite with zinc and fluoride improves mechanical and biological properties of hydroxyapatite [J]. Progress in Natural Science: Materials International, 2014, 24: 340−349.

[26] CANDIDATO R T Jr, SERGI R, JOUIN J, NOGUERA O, PAWŁOWSKI L. Advanced microstructural study of solution precursor plasma sprayed Zn doped hydroxyapatite coatings [J]. Journal of the European Ceramic Society 2018, 38: 2134−2144.

[27] KHALID M, MUJAHID M, NUSAIR A K, RAWAT R S. Dip coating of nano hydroxyapatite on titanium alloy with plasma assisted γ-alumina buffer layer: A novel coating approach [J]. Journal of Material Science and Technology, 2013, 29: 557−564.

[28] CATAURO M, BOLLINO F, GIOVANARDI R, VERONESI P. Modification of Ti6Al4V implant surfaces by biocompatible TiO_2/PCL hybrid layers prepared via sol−gel dip coating: Structural characterization, mechanical and corrosion behavior [J]. Journal of Material Science and Engineering C, 2017, 74: 501−507.

[29] MAVIS B, TAŞ C A. Dip coating of calcium hydroxyapatite on Ti−6Al−4V substrates [J]. Journal of the American Ceramic Society, 2000, 83: 989−991.

[30] IQBAL N, KADIR M R A. Microwave synthesis and antibacterial studies of bioceramics doped with antibacterial metal [C]//AIP Conference Proceedings. 2017, 1901: 100009.

[31] KOKUBO T, TAKADAMA H. How useful is SBF in predicting in vivo bone bioactivity? [J]. Biomaterials, 2006, 27: 2907−2915.

[32] GAO Y, ZHAO L, YAO X, HANG R, ZHANG X, TANG B. Corrosion behavior of porous ZrO_2 ceramic coating on AZ31B magnesium alloy [J]. Surface Coatings and Technology, 2018, 349: 434−441.

[33] AKHBAR S, SUBUKI I, SHARUDIN R W. Performance of polycaprolactone/hydroxyapatite (PCL/HA) composite blended by ultrasound assisted melt blending [J]. Journal of Mechanical Engineering, 2018, SI 5(5): 235−250.

[34] SHI Z, LIU M, ATRENS A. Measurement of the corrosion rate of magnesium alloys using Tafel extrapolation [J]. Corrosion Science, 2010, 52(2): 579−588.

[35] ABDEL-AAL E A, DIETRICH D, STEINHAEUSER S, WIELAGE B. Electrocrystallization of nanocrystallite calcium phosphate coatings on titanium substrate at different current densities [J]. Surface Coatings Technology, 2008, 202: 5895−5900.

[36] GU X N, ZHENG W, CHENG Y, ZHENG Y F. A study on alkaline heat treated Mg−Ca alloy for the control of the biocorrosion rate [J] Acta Biomaterials, 2009, 5(7): 2790−2799.
[37] BAKHSHESHI-RAD H R, HAMZAH E, DAROONPARVAR M, YAJID M A M, MEDRAJ M. Fabrication and corrosion behavior of Si/HA nano-composite coatings on biodegradable Mg−Zn−Mn−Ca alloy [J]. Surface and Coatings Technology, 2014, 258: 1090−1099.
[38] FEKRY A M, EL-SHERIF R M. Electrochemical corrosion behavior of magnesium and titanium alloys in simulated body fluid [J]. Electrochimica Acta, 2009, 54: 7280−7285.

掺锌羟基磷灰石−沸石/聚己内酯复合材料作为镁基体涂层提高其体外腐蚀和抗菌性能

Nida IQBAL[1], Saman IQBAL[2], Tanveer IQBAL[3], H. R. BAKHSHESHI-RAD[4], Ahmed ALSAKKAF[5], Ahmad KAMIL[6], Mohammed Rafiq ABDUL KADIR[7], Mohd Hasbullah IDRIS[5], H. Balaji RAGHAV[8]

1. Biomedical Engineering Centre, University of Engineering and Technology, Kala Shah Kaku (KSK) Campus, Lahore, Pakistan;
2. Department of Physics, University of the Punjab, Quaid-e-Azam Campus, Labore, Pakistan;
3. Department of Chemical Polymer & Composite Material Engineering, University of Engineering and Technology, Kala Shah Kaku (KSK) New Campus, Lahore, Pakistan;
4. Advanced Materials Research Center, Department of Materials Engineering, Najafabad Branch, Islamic Azad University, Najafabad, Iran;
5. School of Mechanical Engineering, Faculty of Engineering, Universiti Teknologi Malaysia, Johor, Malaysia;
6. Kulliyyah of Science, International Islamic University Malaysia, Bandar Indera Mahkota Campus, Jalan Sultan Ahmad Shah, 25200 Kuantan, Pahang Darul Makmur, Malaysia;
7. School of Biomedical Engineering and Health Sciences, Faculty of Engineering, Universiti Teknologi Malaysia, Johor, Malaysia;
8. Tissue Engineering Group (TEG), National Orthopaedic Centre of Excellence in Research and Learning (NOCERAL), Department of Orthopaedic Surgery, Faculty of Medicine, University of Malaya, 50603 Lembah Pantai, Kuala Lumpur, Malaysia

摘　要：开发掺锌羟基磷灰石−沸石(ZnHA−Zeo)和聚己内酯(PCL)复合涂层，以提高镁基体的耐腐蚀性能和抗菌性能。采用浸涂技术在室温下将 ZnHA−Zeo/PCL 涂覆在镁基体上，对样品进行场发射扫描电子显微镜(FESEM)、X 射线衍射(XRD)、傅里叶变换红外光谱(FTIR)、能量色散 X 射线光谱(EDX)和抗菌电位测试。结果表明，复合涂层由羟基磷灰石 (HA)、磷钙锌石(scholzite)、沸石和 PCL 相组成。EDX 谱显示钙(Ca)、硅(Si)、铝(Al)、锌(Zn)、磷(P)和氧(O)元素的存在。复合涂层表面的显微形貌为球形，厚度为 226~260 μm。掺锌 HA−Zeo 复合涂层具有较高的耐蚀性，对镁基体表面提供足够的保护，使其不被电流腐蚀。与未掺杂的涂层相比，掺锌 HA−Zeo 涂层对大肠杆菌具有更好的抗菌活性。综合结果表明，ZnHA−Zeo 涂层不仅具有良好的耐腐蚀性能，而且具有良好的抗菌性能，可作为种植体应用的理想材料。

关键词：可降解镁合金；生物陶瓷涂层；耐腐蚀性；抗菌活性

(Edited by Bing YANG)